QUANTUM COMPUTING

Hartree-Fock on a superconducting qubit quantum computer

Google AI Quantum and Collaborators*†

The simulation of fermionic systems is among the most anticipated applications of quantum computing. We performed several quantum simulations of chemistry with up to one dozen qubits, including modeling the isomerization mechanism of diazene. We also demonstrated error-mitigation strategies based on *N*-representability that dramatically improve the effective fidelity of our experiments. Our parameterized ansatz circuits realized the Givens rotation approach to noninteracting fermion evolution, which we variationally optimized to prepare the Hartree-Fock wave function. This ubiquitous algorithmic primitive is classically tractable to simulate yet still generates highly entangled states over the computational basis, which allowed us to assess the performance of our hardware and establish a foundation for scaling up correlated quantum chemistry simulations.

The prediction of molecular properties and chemical reactions from ab initio quantum mechanics has emerged as one of the most promising applications of quantum computing (*1*). This fact is due both to the commercial value of accurate simulations as well as the relatively modest number of qubits required to represent interesting instances. However, as the age of "quantum supremacy" dawns (*2*), so has a more complete appreciation of the challenges required to scale such computations to the classically intractable regime using near-term intermediate scale quantum (NISQ) devices. Achieving that objective will require further algorithmic innovations, hardware with more qubits and low error rates, and more effective error-mitigation strategies. Here, we report a variational quantum eigensolver (VQE) (*3*) simulation of molecular systems with progress in all three directions.

We used the Google Sycamore quantum processor to simulate the binding energy of hydrogen chains as large as H_{12}, as well as a chemical reaction mechanism (the isomerization of diazene). The Sycamore quantum processor consists of a two-dimensional array of 54 transmon qubits (*2*). Each qubit is tunably coupled to four nearest neighbors in a rectangular lattice. Our largest simulations used a dozen qubits—twice the size as the largest prior quantum simulations of chemistry (*4*)—and required only nearest-neighbor coupling (Fig. 1). Prior simulations of chemistry on superconducting qubit devices and trapped ion systems demonstrated the possibility of error mitigation through VQE (*4*–*10*), albeit on a small scale. We demonstrated that within the model, achieving chemical accuracy through VQE is possible for intermediate-scale problems when combined with effective error mitigation strategies. Furthermore, we argue that the circuit ansatz we used for VQE is especially appealing as a benchmark for chemistry.

We simulated quantum chemistry in a second-quantized representation in which the state of each of N qubits encoded the occupancy of an orbital basis function. We used what are commonly referred to as "core orbitals" as the initial orbitals (shown for H_{12} in Fig. 1A, left), which are the eigenfunctions of the molecular Hamiltonian without the electron-electron interaction term. The goal of this experiment was to use a quantum computer to implement the Hartree-Fock procedure, which is a method for obtaining the best single-particle orbital functions assuming each electron feels the average potential generated from all the other electrons. This assumption is enforced by constraining the wave function to be a product of one-particle functions, which has been appropriately antisymmetrized to satisfy the Pauli exclusion principle. An initial guess for the Hartree-Fock state, from which we can optimize the orbitals, was obtained by filling the lowest-energy $\eta/2$ orbitals, each with a spin-up electron and a spin-down electron, where η is the number of electrons. Because we simulated the singlet ground state for all molecules considered here, there is no spin component to the mean-field approximation; thus, we only needed to explicitly simulate the $\eta/2$ spin-up electrons.

By performing a unitary rotation of the initial (core) orbital basis $\varphi_p(r)$, one can obtain a new valid set of orbitals $\tilde{\varphi}_p(r)$ as a linear combination of the initial ones:

$$\tilde{\varphi}_p(r) = \sum_{q=1}^{N} [e^{\kappa}]_{pq} \varphi_q(r) \qquad (1)$$

where κ is an $N \times N$ anti-Hermitian matrix and $[e^{\kappa}]_{pq}$ is the p, q element of the matrix exponential of κ. A result attributable to Thouless (*11*) is that one can express the unitary that applies this basis rotation to the quantum state as time-evolution under a noninteracting fermion Hamiltonian. Specifically, if we take $a_p^\dagger$ and a_p to be fermionic creation and annihilation operators, respectively, for the core orbital $\varphi_p(r)$, then we can parameterize $|\psi_\kappa\rangle$, an antisymmetric product state in the new basis $\tilde{\varphi}_p(r)$, as noninteracting fermion dynamics from a computational basis state $|\eta\rangle = a_\eta^\dagger \cdots a_1^\dagger |0\rangle$ in the core orbital basis:

$$|\psi_\kappa\rangle = U_\kappa |\eta\rangle,$$
$$U_\kappa = \exp\left(\sum_{p,q=1}^{N} \kappa_{pq} a_p^\dagger a_q\right) \qquad (2)$$

Such states are referred to as Slater determinants.

To complete the accurate preparation of Hartree-Fock states, we implemented variational relaxation of the κ parameters to minimize the energy of $|\psi_\kappa\rangle$ starting from the optimal κ determined by solving the Hartree-Fock equations classically. This is an idealized implementation of VQE that allowed us to demonstrate error mitigation of coherent errors through variational relaxation. We defined the Hartree-Fock state $|\psi_{HF}\rangle$ to be the lowest-energy Slater determinant for the molecular Hamiltonian H

$$|\psi_{HF}\rangle = |\psi_{\kappa^*}\rangle, \kappa^* = \arg\min_\kappa \langle\psi_\kappa|H|\psi_\kappa\rangle \qquad (3)$$

We applied U_κ to $|\eta\rangle$ using our quantum computer and then performed the optimization over κ through feedback from a classical optimization routine. The energy decreased because the initial core orbitals were obtained by ignoring the electron-electron interaction and variational relaxation compensates for coherent errors. Because the generator for U_κ corresponds to a noninteracting fermion Hamiltonian, its action on a product state in second quantization can be classically simulated in $O(N^3)$ by diagonalizing the one-body operator, and in some cases, the Hartree-Fock procedure can be made to converge with even lower complexity. Despite this, we argue that this procedure is still a compelling experiment for a quantum computer.

The Hartree-Fock state is usually the initial state for classical correlated electronic structure calculations such as coupled cluster and configuration interaction methods, as well as for many quantum algorithms for chemistry. Thus, often one chooses to work in the molecular orbital basis, which is defined so that the Hartree-Fock state is a computational basis state. However, the molecular orbital basis Hamiltonian has a large number of terms that can be challenging to simulate and measure with low complexity. Accordingly, the most efficient quantum algorithms for chemistry (*12*–*15*) require that one perform the simulation in more structured bases with asymptotically fewer terms (*16*–*18*), necessitating that U_{κ^*} is applied explicitly at the beginning of the computation. Even when simulating chemistry

*Corresponding author. Email: nickrubin@google.com (N.C.R.); babbush@google.com (R.J.B.) †Google AI Quantum authors, collaborators, and affiliations are listed in the supplementary materials.

in an arbitrary basis, the most efficient strategies are based on a tensor factorization of the Hamiltonian that requires many applications of U_κ to simulate (*19*, *20*). Exploiting this tensor factorization with basis rotations is also key to the most efficient strategy for measuring $\langle H \rangle$ in variational algorithms and requires implementing U_κ before measurement (*21*).

We used this variational ansatz based on basis rotations to benchmark the Sycamore processor for linear hydrogen chains of length 6, 8, 10, and 12 and two pathways for diazene bond isomerization. We modeled hydrogen chains of length N with N qubits. Our simulations required N qubits to simulate $2N$ spin orbitals because of the constraint that the α–spin orbitals have the same spatial wave function as that of the β–spin orbitals. For diazene, we required 10 qubits after preprocessing. The hydrogen chains are a common benchmark in electronic structure (*22*–*24*), and the diazene bond isomerization provides a system in which the required accuracy is more representative of typical electronic structure problems and has been used as a benchmark for coupled-cluster methods (*25*). For the diazene isomerization, our goal was to resolve the energetic difference between the transition states of two competing mechanisms, requiring accuracy of about 40 millihartree. This objective differs from prior quantum simulations of chemistry, which have focused on bond dissociation curves (*4*–*7*).

One motivation for this work was to calibrate and validate the performance of our device in realizing an important algorithmic primitive for quantum chemistry and lattice model simulation. Our experiment was also appealing for benchmarking purposes because the circuits we explored generated highly entangled states but with a special structure that enabled the efficient measurement of fidelity and the determination of systematic errors. Further motivation was to implement the largest variational quantum simulation of chemistry so that it would be possible to better quantify the current gap between the capabilities of NISQ devices and real applications. Even though the Hartree-Fock ansatz is efficient to simulate classically, the circuits in our experiment are far more complex than prior experimental quantum simulations of chemistry. Last, the structure of the Hartree-Fock state enabled us to sample the energy and gradients of the variational ansatz with fewer measurements than typically would be required, allowing us to focus on other aspects of simulating chemistry at scale, such as the effectiveness of various types of error mitigation. Thus, our choice to focus on Hartree-Fock for this experiment embraces the notion that we should work toward valuable quantum simulations of chemistry by first scaling up important components of the exact solution (such as error-mitigation strategies and basis rotations) in a fashion that enables us to completely understand and perfect those primitives.

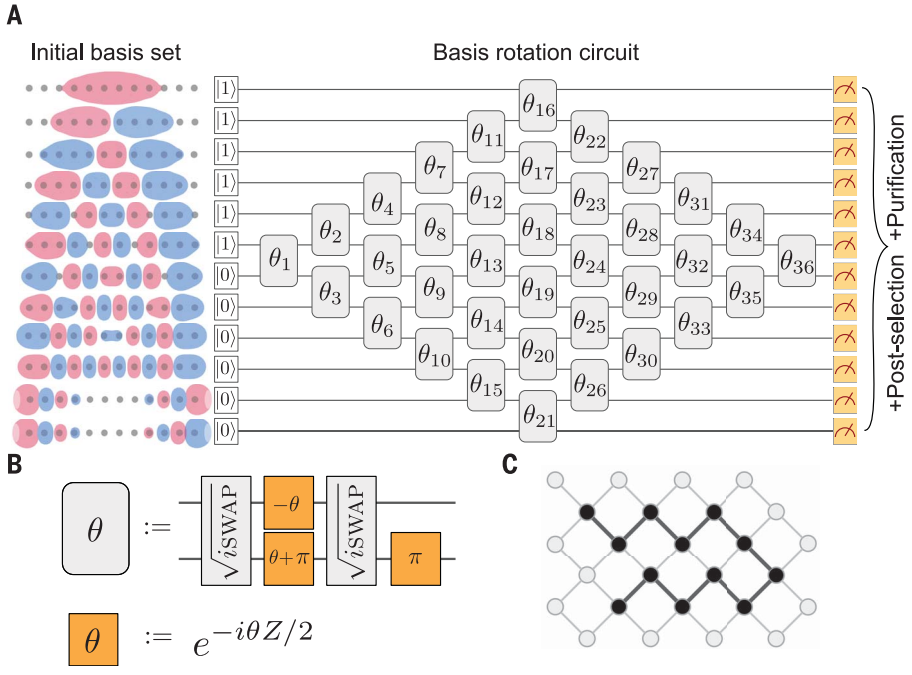

Fig. 1. Basis rotation circuit and compilation. (**A**) To the left of the circuit diagram are the initial orbitals for the H_{12} chain with atom spacings of 1.3 Å, obtained by diagonalizing the Hamiltonian, ignoring electron-electron interactions. The circuit diagram depicts the basis rotation ansatz for a linear chain of 12 hydrogen atoms. Each gray box with a rotation angle θ represents a Givens rotation gate. (**B**) Compilation of the Givens rotation gate to $\sqrt{i\mathrm{SWAP}}$ gates and single-qubit gates that can be realized directly in hardware. The H_{12} circuit involves 72 $\sqrt{i\mathrm{SWAP}}$ gates and 108 single-qubit Z rotation gates with a total of 36 variational parameters. (**C**) Depiction of a 12-qubit line on a subgrid of the entire 54-qubit Sycamore device. All circuits only require gates between pairs of qubits that are adjacent in a linear topology.

Variational algorithms are specified in the form of a functional minimization. This minimization has three main components: ansatz specification in the form of a parameterized quantum circuit (the function), observable estimation (the functional), and outer-loop optimization (the minimization). Each component is distinctively affected by our choice to simulate a model corresponding to noninteracting fermion wave functions. Symmetries built into this ansatz allowed for reduction of the number of qubits required to simulate molecular systems, a reduction in the number of measurements needed to estimate the energy, and access to the gradient without additional measurements beyond those required for energy estimation. Details on how we realized Hartree-Fock with VQE are available in the supplementary materials, section A.

The unitary in Eq. 2 can be compiled exactly (without Trotterization) by using a procedure based on Givens rotations. This strategy was first suggested for quantum computing in work on linear optics in (*26*) and later in the context of fermionic simulations in (*27*). We implemented these basis rotations using the optimal compilation of (*28*), which has gate depth $N/2$ and requires only $\eta(N - \eta)$ two-qubit "Givens rotation" gates on a linearly connected architecture, giving one rotation for each element in the unitary basis change. These Givens rotation gates were implemented by decomposition into two $\sqrt{i\mathrm{SWAP}}$ gates and three Rz gates. In Fig. 1, we depict the basis change circuit for the H_{12} chain, which has a diamond-shaped structure. We further review the compilation of these circuits in the supplementary materials, section B.

The average energy of any molecular system can be evaluated with knowledge of the one-particle reduced-density matrix (1-RDM), $\langle a_p^\dagger a_q \rangle$, and the two-particle reduced-density matrix (2-RDM), $\langle a_p^\dagger a_q^\dagger a_r a_s \rangle$. In general, it is not possible to exactly reconstruct the 2-RDM from knowledge of just the 1-RDM. However, for single-Slater determinants (as in our Hartree-Fock experiment), the 2-RDM is completely determined by the 1-RDM (*29*):

$$\left\langle a_p^\dagger a_q^\dagger a_r a_s \right\rangle = \left\langle a_p^\dagger a_s \right\rangle \left\langle a_q^\dagger a_r \right\rangle - \left\langle a_q^\dagger a_s \right\rangle \left\langle a_p^\dagger a_r \right\rangle \quad (4)$$

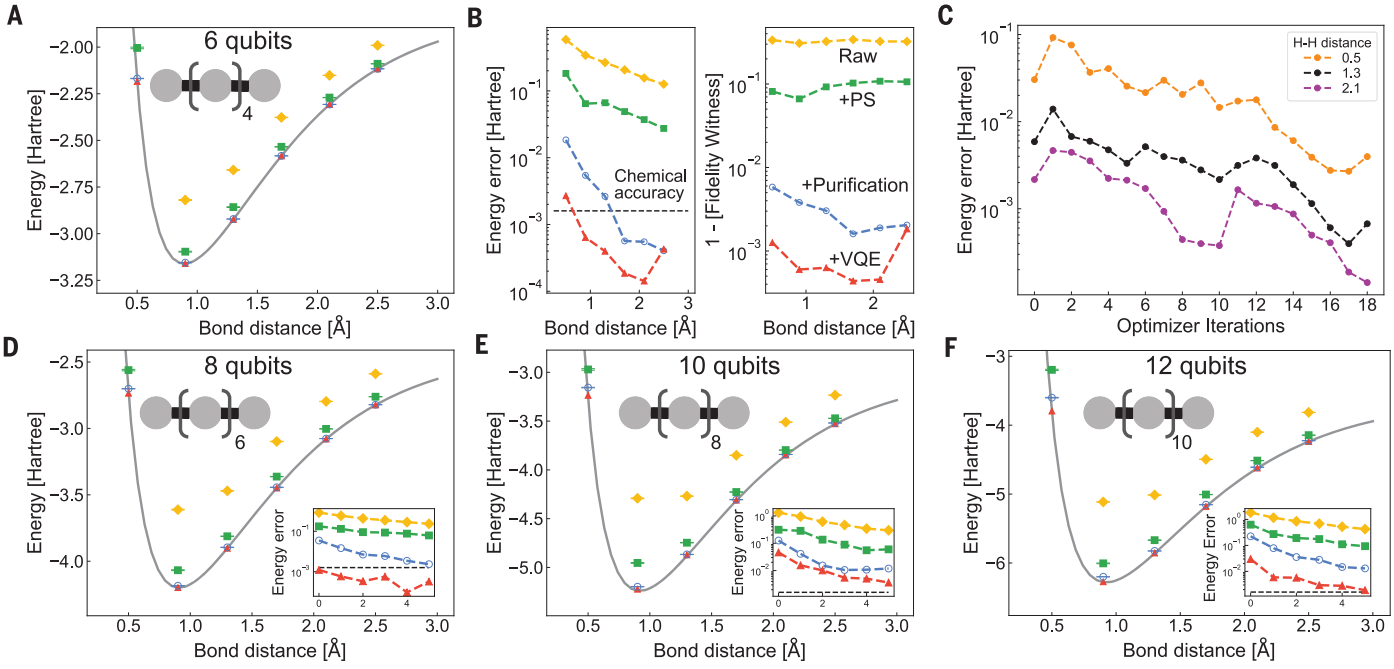

Fig. 2. Static and VQE performance on hydrogen chains. Binding curve simulations for H_6, H_8, H_{10}, and H_{12} with various forms of error mitigation. (**A** and **D** to **F**) Comparison of Sycamore's raw performance (yellow diamonds) with postselection (green squares), purification (blue circles), and error-mitigated combined with variational relaxation (red triangles). For all hydrogen systems, the raw data at 0.5-Å bond length is off the top of the plot. The yellow, green, and blue points were calculated by using the optimal basis rotation angles computed from a classical simulation; thus, the variational optimization shown here is only used to correct systematic errors in the circuit realization. (**B**) The absolute error and infidelity for the H_6 system. For all points, we calculated a fidelity witness described in the supplementary materials, section D. The error bars for all points were computed by estimating the covariance between simultaneously measured sets of 1-RDM elements and resampling those elements under a multivariate Gaussian model. Energies from each sample were tabulated, and the standard deviation is used as the error bar. The "+PS" means applying postselection to the raw data, "+Purification" means applying postselection and McWeeny purification, and "+VQE" means postselection, McWeeny purification, and variational relaxation. (**C**) Optimization traces for three H_6 geometries (bond distances of 0.5, 1.3, and 2.1 Å). All optimization runs used between 18 and 30 optimization. The lowest-energy solution from the optimization trace was reported.

Thus, in our experiment we only needed to sample the 1-RDM to estimate the energy. Because the 2-RDM has quadratically more elements than the 1-RDM, this approach is a substantial simplification. We measured the 1-RDM using a protocol described in the supplementary materials, section C. This protocol enabled us to optimally parallelize measurement of all N^2 1-RDM elements with $N + 1$ distinct circuits. For each distinct circuit, we made 250,000 measurements.

We performed two types of error mitigation on our measured data: postselection on particle number (conserved in basis rotations) and pure-state projection. To apply postselection, we modified our circuits by first rotating into a basis that diagonalizes $a_p^\dagger a_q + a_q^\dagger a_p$ for N different pairs of p and q so that these elements could be sampled at the same time as the total particle-number operator. Following the strategy in the supplementary materials, section C, this measurement was accomplished at the cost of two T gates and one $\sqrt{i\mathrm{SWAP}}$ gate per pair of qubits. We then postselected to discard measurements where the total number of excitations changed from $\eta/2$.

For pure-state purification, we leveraged the fact that the 1-RDM of any single-Slater determinant wave function ψ_κ has eigenvalues restricted to be 0 and 1 (*30*). We performed projection back to the pure set of 1-RDMs using a technique known as McWeeny purification (*29*). Details on the procedure and sampling bounds for guaranteeing that the procedure has a fixed-point 1-RDM corresponding to a Slater determinant can be found in the supplementary materials, section E. Although McWeeny purification only works for Slater determinant wave functions, pure-state N-representability conditions are known for more general systems (*31*), and we expect that a computational procedure similar to enforcing ensemble constraints could be used (*32*, *33*).

A variety of circuit optimization techniques based on gradient and gradient-free methods have been proposed in the context of NISQ algorithms. We developed an optimization technique that exploits local gradient and Hessian information in a fashion that is distinctive to the Hartree-Fock model. It is based on a proposal for iterative construction of a wave function to satisfy the Brillouin condition for a single-particle model (*34*). Our optimization protocol used the property that at a local optima, the commutator of the Hamiltonian H with respect to any generator of rotation G is zero—$\langle\psi|[H, G]|\psi\rangle = 0$—and sequential basis change circuits can be concatenated into a single basis change circuit ($U_a U_b = U_{ab}$). Using these relations and taking $G = \sum_{pq} \kappa_{pq} a_p^\dagger a_q$, as in our experiment, the double commutator $\langle\psi|[H, G], G|\psi\rangle$ determined an augmented Hessian (matrix of derivatives) that we could use to iteratively update the wave function so that the first-order condition was approximately satisfied. Regularization was added by limiting the size of update parameters (*35*). Details are provided in the supplementary materials, section H.

As a benchmark, we studied symmetrically stretched hydrogen chains of lengths 6, 8, 10, and 12 atoms (Fig. 2). The initial parameters were set to the parameters obtained by solving the Hartree-Fock equations on a classical computer. The data from the quantum computer were plotted along with classical Hartree-Fock results, showing better and better agreement as we added postselection, postselection and purification, and then error-mitigated variational relaxation. The 6- and 8-qubit data achieved chemical accuracy after VQE, and even the 12-qubit data followed the expected energy closely. The error data in Fig. 2B and

the other inserts show a large and consistent decrease, about a factor of 100, when using these protocols. The substantial decrease in error when using a modest number of VQE iterations is shown in Fig. 2C.

A fidelity witness can be efficiently computed from the experimental data (supplementary materials, section D.2) (*36*). This value is a lower bound to the true fidelity and thus potentially loose when fidelity is small. However, this fidelity generally tracked the measured errors (Fig. 2B). As shown in Table 1, fidelity increased as we added various forms of error mitigation, starting in the left column, where the optimal angles were computed classically. Uncertainties in the last digit, indicated in parentheses, were calculated by means of the procedure described in the supplementary materials, section C.5. The first column of Table 1 is an estimate of the fidelity based on multiplying the fidelity for all the gates and readout assuming 99.5% fidelity for single qubit gates, 99% fidelity for two-qubit gates, and 97% fidelity for readout. We see that this estimate qualitatively follows the "raw" fidelity witness estimates, except when the witness value is very small. For all hydrogen systems studied, we observed drastic fidelity improvements, with combined error mitigation.

We simulated two isomerization pathways for diazene, marking the first time that a chemical reaction mechanism has been modeled by using a quantum computer. Hartree-Fock theory reverses the order of the transition states; however, we focused on the accuracy of the computation with respect to the simulated model. Correctly identifying this pathway requires resolving the energy gap of 40 millihartree between the two transition states. The pathways correspond to the motion of the hydrogen in the process of converting *cis*-diazene to *trans*-diazene. One mechanism is in-plane rotation of a hydrogen, and the other is an out-of-plane rotation corresponding to rotation of the HNNH dihedral angle. VQE-optimized data simulating nine points along the reaction coordinates for in-plane and out-of-plane rotation of hydrogen are shown in Fig. 3. For all points along the reaction coordinate, the initial parameter setting was the solution to the Hartree-Fock equations. VQE produced 1-RDMs with an average fidelity greater than 0.98 after error mitigation. Our full error-mitigation procedure again substantially improved the accuracy of our calculation.

Our VQE calculations on diazene predicted the correct ordering of the transition states to within the chemical model with an energy gap of 41 ± 6 millihartree, and the true gap is 40.2 millihartree. We provide a more detailed analysis of the error mitigation performance on the diazene circuits in the supplementary materials, section F, considering that the $\sqrt{i\mathrm{SWAP}}$ gates we used had a residual CPHASE ($\pi/24$) and Rz gates had stochastic control angles. This simulation reinforced VQE's ability to mitigate systematic errors at the scale of 50 $\sqrt{i\mathrm{SWAP}}$ gates and over 80 Rz gates.

In this work, we took a step toward answering the question of whether NISQ computers can offer quantum advantage for chemical simulation by studying VQE performance on basis rotation circuits that are widely used in quantum algorithms for fermionic simulation. The considered ansatz afforded ways to minimize the resource requirements for VQE and study device performance for circuits that are similar to those needed for full Hamiltonian simulation. These basis rotation circuits also made an attractive benchmark because of their prevalence, optimal known compilation, and ability to extract fidelity and fidelity witness

Table 1. Average-fidelity lower bounds for hydrogen chain calculations. We report values of the fidelity witness from (*36*), averaged across H–H separations of {0.5, 0.9, 1.3, 1.7, 2.1, 2.5} Å, starting from circuits with the theoretically optimal variational parameters (κ). "Estimate" corresponds to an estimate of the fidelity derived by multiplying gate errors assuming 0.5% single-qubit gate error, 1% two-qubit gate error, and 3% readout error. "Raw" corresponds to fidelities from constructing the 1-RDM without any error mitigation. "+PS" corresponds to fidelities from constructing the 1-RDM with postselection on particle number. "+Pure" corresponds to fidelities from constructing the 1-RDM with postselection and applying purification as postprocessing. "+VQE" corresponds to fidelities from using all previously mentioned error mitigation techniques in conjunction with variational relaxation. Numbers in parentheses are the uncertainties of the last, preceding digit. For small values (such as the "raw" value for H_{12}), we expect that the fidelity lower-bound is more likely to be loose.

System	Estimate	Raw	+PS	+Pure	+VQE
H_6	0.571	0.674(2)	0.906(2)	0.9969(1)	0.99910(9)
H_8	0.412	0.464(2)	0.827(2)	0.9879(3)	0.99911(8)
H_{10}	0.277	0.316(2)	0.784(3)	0.9704(5)	0.9834(4)
H_{12}	0.174	0.010(2)	0.654(3)	0.9424(9)	0.9913(3)

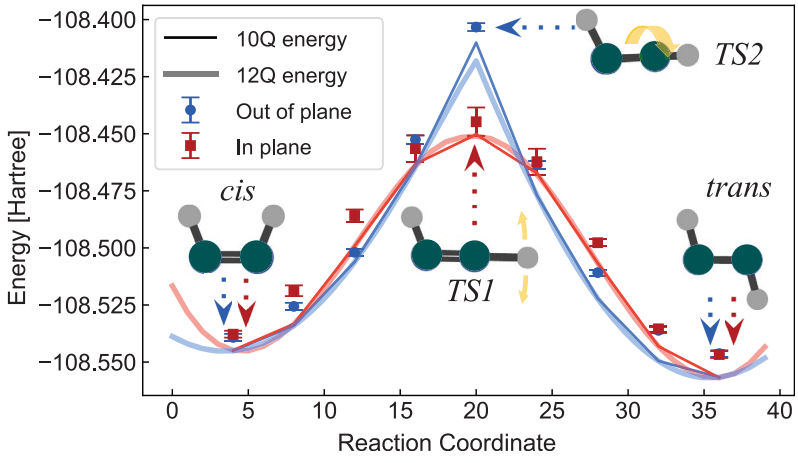

Fig. 3. VQE performance on distinguishing the mechanism of diazene isomerization. Hartree-Fock curves for diazene isomerization between cis and trans configurations. TS1 and TS2 are the transition states for the in-plane and out-of-plane rotation of the hydrogen, respectively. The yellow arrows on TS1 and TS2 indicate the corresponding reaction coordinate. The solid curve is the energy obtained from optimizing a 10-qubit problem generated by freezing the core orbitals generated from two self-consistent field cycles. The transparent lines of the same color are the full 12-qubit system, indicating that freezing the lowest two levels does not change the characteristics of the model chemistry. Nine points along the reaction paths are simulated on Sycamore by using VQE. We allowed the optimizer 30 iterations for all points, except for fifth and sixth points from the left of the in-plane rotation curve, for which we allowed 60 steps. The error bars for all points were computed by estimating the covariance between simultaneously measured sets of 1-RDM elements and resampling those elements under a multivariate Gaussian model. Energies from each sample were tabulated, and the standard deviation is used as the error bar. No purification was applied for the computation of the error bar. If purification is applied, the error bars become smaller than the markers. Each basis rotation for diazene contains 50 $\sqrt{i\mathrm{SWAP}}$ gates and 80 Rz gates.

values and because they parameterize a continuous family of analytically solvable circuits that demonstrate a high degree of entanglement. The circuits also serve as a natural progression toward more correlated ansatz such as a generalized swap network (*28*) or a non–particle-conserving circuit ansatze followed by particle-number projection.

We demonstrated the performance of two error-mitigation techniques on basis rotation circuit fidelity. The first is postselection on total occupation number when measuring all elements of the 1-RDM. This step was accomplished by permuting the basis rotation circuit so that all measurements involved estimating nearest-neighbor observables and measuring each pair of observables so that the total occupation number is preserved. The second is the application of McWeeny purification as a postprocessing step. The energy improvements from projecting back to the pure-state N-representable manifold was evidence that generalized pure-state N-representability conditions would be instrumental in making NISQ chemistry computations feasible. This underscores the importance of developing procedures for applying pure-state N-representability conditions in a more general context. The postselection and RDM measurement techniques can be generalized to measuring all 1-RDM and 2-RDM elements when considering a less restrictive circuit ansatz by permuting the labels of the fermionic modes. For ansatz such as the generalized swap network (*28*), the circuit structure would not change, only the rotation angles. Thus, the measurement schemes presented here are applicable in the more general case. Furthermore, it is important to understand the performance of these error-mitigation techniques when combined with alternatives such as noise extrapolation (*37*).

Last, we were able to show further evidence that variational relaxation effectively mitigates coherent errors that arise in the implementation of physical gates. The performance of our problem-specific optimization strategy motivates the study of iterative wave function constructions (*38*) in a more general setting. The combination of these error-mitigation techniques with VQE unambiguously resolved a chemical mechanism to within the model chemistry by using a quantum computation. It is still an open question whether NISQ devices will be able to simulate challenging quantum chemistry systems, and it is likely that major innovations will be required. However, we find the accuracy of these experiments and the effectiveness of these error-mitigation procedures to be an encouraging signal of progress in that direction.

REFERENCES AND NOTES

1. A. Aspuru-Guzik, A. D. Dutoi, P. J. Love, M. Head-Gordon, *Science* **309**, 1704–1707 (2005).
2. F. Arute *et al.*, *Nature* **574**, 505–510 (2019).
3. A. Peruzzo *et al.*, *Nat. Commun.* **5**, 4213 (2014).
4. A. Kandala *et al.*, *Nature* **549**, 242–246 (2017).
5. P. J. J. O'Malley *et al.*, *Phys. Rev. X* **6**, 031007 (2016).
6. C. Hempel *et al.*, *Phys. Rev. X* **8**, 031022 (2018).
7. A. Kandala *et al.*, *Nature* **567**, 491–495 (2019).
8. J. I. Colless *et al.*, *Phys. Rev. X* **8**, 011021 (2018).
9. S. E. Smart, D. A. Mazziotti, *Phys. Rev. A* **100**, 022517 (2019).
10. R. Sagastizabal *et al.*, *Phys. Rev. A* **100**, 010302 (2019).
11. D. J. Thouless, *Nucl. Phys.* **21**, 225–232 (1960).
12. G. H. Low, N. Wiebe, arXiv:1805.00675 [quant-ph] (2018).
13. R. Babbush, D. W. Berry, J. R. McClean, H. Neven, *npj Quantum Information* **5**, 92 (2019).
14. A. M. Childs, Y. Su, M. C. Tran, N. Wiebe, S. Zhu, arXiv:1912.08854 [quant-ph] (2019).
15. R. Babbush *et al.*, *Phys. Rev. X* **8**, 041015 (2018).
16. R. Babbush *et al.*, *Phys. Rev. X* **8**, 011044 (2018).
17. S. R. White, *J. Chem. Phys.* **147**, 244102 (2017).
18. J. R. McClean *et al.*, arXiv:1909.00028 [quant-ph] (2019).
19. M. Motta *et al.*, arXiv:1808.02625 [physics.comp-ph] (2018).
20. D. Berry, C. Gidney, M. Motta, J. McClean, R. Babbush, *Quantum* **3**, 208 (2019).
21. W. J. Huggins *et al.*, arXiv:1907.13117 [quant-ph] (2019).
22. M. Motta *et al.*, *Phys. Rev. X* **7**, 031059 (2017).
23. P. A. Limacher *et al.*, *J. Chem. Theory Comput.* **9**, 1394–1401 (2013).
24. J. Hachmann, W. Cardoen, G. K.-L. Chan, *J. Chem. Phys.* **125**, 144101 (2006).
25. R. K. Chaudhuri, K. F. Freed, S. Chattopadhyay, U. Sinha Mahapatra, *J. Chem. Phys.* **128**, 144304 (2008).
26. M. Reck, A. Zeilinger, H. J. Bernstein, P. Bertani, *Phys. Rev. Lett.* **73**, 58–61 (1994).
27. D. Wecker *et al.*, *Phys. Rev. A* **92**, 062318 (2015).
28. I. D. Kivlichan *et al.*, *Phys. Rev. Lett.* **120**, 110501 (2018).
29. R. McWeeny, *Rev. Mod. Phys.* **32**, 335–369 (1960).
30. A. J. Coleman, *Rev. Mod. Phys.* **35**, 668–686 (1963).
31. D. A. Mazziotti, *Phys. Rev. A* **94**, 032516 (2016).
32. N. C. Rubin, R. Babbush, J. McClean, *New J. Phys.* **20**, 053020 (2018).
33. A. A. Klyachko, *J. Phys.* **36**, 72 (2006).
34. W. Kutzelnigg, *Chem. Phys. Lett.* **64**, 383–387 (1979).
35. Q. Sun, arXiv:1610.08423 [physics.chem-ph] (2016).
36. M. Gluza, M. Kliesch, J. Eisert, L. Aolita, *Phys. Rev. Lett.* **120**, 190501 (2018).
37. K. Temme, S. Bravyi, J. M. Gambetta, *Phys. Rev. Lett.* **119**, 180509 (2017).
38. H. R. Grimsley, S. E. Economou, E. Barnes, N. J. Mayhall, *Nat. Commun.* **10**, 3007 (2019).
39. J. R. McClean *et al.*, arXiv:1710.07629 [quant-ph] (2017).
40. F. Arute *et al.*, Hartree-fock on a superconducting qubit quantum computer. Dryad, Dataset (2020); doi:10.5061/dryad.2jm63xsm2.

ACKNOWLEDGMENTS

D.B. is a CIFAR Associate Fellow in the Quantum Information Science Program. **Funding:** This work was supported by Google. **Competing interests:** The authors declare no competing interests. **Author contributions:** N.C.R. designed the experiment. C.N. assisted with data collection. Z.J., V.S., and N.W. assisted with analytical calculations and gate synthesis. N.C.R. and R.J.B. wrote the paper. Experiments were performed by using a quantum processor that was recently developed and fabricated by a large effort involving the entire Google Quantum team. **Data and materials availability:** The code used for this experiment and a tutorial for running it can be found in the open-source library ReCirq, located at https://github.com/quantumlib/ReCirq (*39*). All data needed to evaluate the conclusions in the paper are present in the paper or the supplementary materials. Data presented in the figures can be found in the Dryad repository (*40*).

SUPPLEMENTARY MATERIALS

science.sciencemag.org/content/369/6507/1084/suppl/DC1
Supplementary Text
Figs. S1 to S11
Tables S1 to S11
References (*41*–*50*)

1 April 2020; accepted 18 June 2020
10.1126/science.abb9811

Hartree-Fock on a superconducting qubit quantum computer

Google AI Quantum and Collaborators

Science **369** (6507), 1084-1089.
DOI: 10.1126/science.abb9811

Twelve-qubit quantum computing for chemistry

Accurate electronic structure calculations are considered one of the most anticipated applications of quantum computing that will revolutionize theoretical chemistry and other related fields. Using the Google Sycamore quantum processor, Google AI Quantum and collaborators performed a variational quantum eigensolver (VQE) simulation of two intermediate-scale chemistry problems: the binding energy of hydrogen chains (as large as H_{12}) and the isomerization mechanism of diazene (see the Perspective by Yuan). The simulations were performed on up to 12 qubits, involving up to 72 two-qubit gates, and show that it is possible to achieve chemical accuracy when VQE is combined with error mitigation strategies. The key building blocks of the proposed VQE algorithm are potentially scalable to larger systems that cannot be simulated classically.

Science, this issue p. 1084; see also p. 1054

Science (print ISSN 0036-8075; online ISSN 1095-9203) is published by the American Association for the Advancement of Science, 1200 New York Avenue NW, Washington, DC 20005. The title *Science* is a registered trademark of AAAS.